



# Repurposing the porous separator from spent Li-ion batteries towards building quasi-solid-state Na-metal batteries with $\text{Na}_{2/3}\text{Ni}_{1/3}\text{Mn}_{2/3}\text{O}_2$ cathode

Shaji Jyothilakshmi<sup>a</sup>, Krishnan Subramanyan<sup>a</sup>, Yun-Sung Lee<sup>b,\*</sup>, Vanchiappan Aravindan<sup>a,\*</sup>

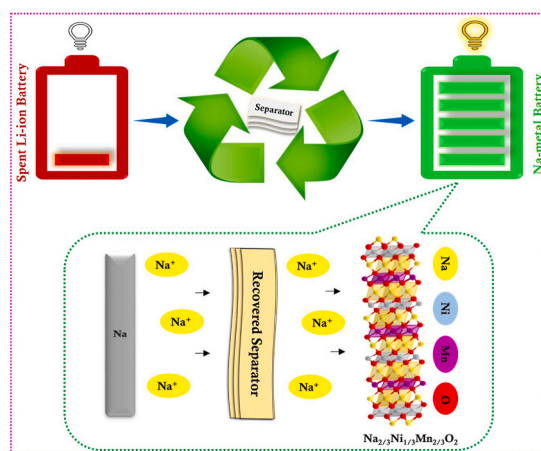
<sup>a</sup> Department of Chemistry, Indian Institute of Science Education and Research (IISER), Tirupati, 517619, India

<sup>b</sup> School of Chemical Engineering, Chonnam National University, Gwang-ju, 61186, Republic of Korea

## HIGHLIGHTS

- Quasi-solid-state Na-metal batteries are fabricated with a membrane from a spent LIB.
- Excellent wettability and liquid uptake are observed in the recovered separator.
- Robust cycling stability is noted for the membrane with  $\text{Na}_{2/3}\text{Ni}_{1/3}\text{Mn}_{2/3}\text{O}_2$  cathode.

## GRAPHICAL ABSTRACT



## ARTICLE INFO

### Keywords:

Na-metal battery  
Recycling  
Spent Li-ion battery  
Separator

## ABSTRACT

Mechanical strength, wettability, and safety are the main contributors to determining the quality of a separator. In this paper, we recycled the separators from spent lithium-ion batteries (LIBs), upcycled them toward developing quasi-solid-state sodium metal batteries, and analyzed their electrochemical performances. An in-depth investigation of the physical properties of the recycled polymer separator (RPS) is performed in terms of wettability, compatibility, and chemical and mechanical stability. In sodium stripping-plating studies, the RPS sustained its integrity and robustness for more than 600 h without causing any failure. Also, we observed the robust electrochemical performance of RPS with carbonate-based electrolyte in a Na/RPS/ $\text{Na}_{2/3}\text{Ni}_{1/3}\text{Mn}_{2/3}\text{O}_2$  cell with an initial reversible capacity of  $\sim 91 \text{ mAh g}^{-1}$ , along with a coulombic efficiency of  $>97\%$  for beyond

\* Corresponding author.

\*\* Corresponding author.

E-mail addresses: [leey@s@chonnam.ac.kr](mailto:leey@s@chonnam.ac.kr) (Y.-S. Lee), [aravind.van@gmail.com](mailto:aravind.van@gmail.com) (V. Aravindan).

<https://doi.org/10.1016/j.jpowsour.2025.237327>

Received 17 June 2024; Received in revised form 2 May 2025; Accepted 8 May 2025

Available online 22 May 2025

0378-7753/© 2025 Elsevier B.V. All rights are reserved, including those for text and data mining, AI training, and similar technologies.

100 cycles. The recycling of LIBs helps effectively utilize dead battery materials and keeps the environment clean and eco-friendly.

## 1. Introduction

Sodium metal batteries (SMB) are a new type of emerging, inexpensive, high-energy-density electrochemical energy storage devices [1, 2]. Owing to the natural abundance of sodium, the sodium-based battery system is considered a promising alternative to lithium batteries. The direct use of sodium metal (Na) has been considered a promising anode for next-generation rechargeable batteries due to its low redox potential ( $-2.714$  V vs. standard hydrogen electrode), high theoretical capacity ( $1165 \text{ mAh g}^{-1}$ ), and cost-effectiveness [1–3]. Moreover, compared with Li-metal batteries/Li-ion batteries (LIBs), Na-based batteries do not have dendritic issues, leading to battery failure and, thereby, explosions. The safety of batteries is the primary and most challenging factor to consider because of fatal accidents. The separators in batteries are an indispensable component that directly affects the safety as well as the electrochemical performance [4,5]. The separator performs as a physical barricade between the positive and negative electrodes, preventing short circuits and facilitating ions to shuttle inside the battery [6–8]. An ideal separator should have excellent ionic conductivity, wettability, and porosity for faster ionic transport with lower internal impedance. The separator's high mechanical and thermal stability improves battery stability and safety. In addition, it has to be chemically inert with other cell components and should have a wide electrochemical stability window to avoid unwanted side reactions that may cause cell degradation. Polymer-based separators are the safest and most widely used ones in commercial batteries [9]. However, due to the improper disposal of dead LIBs, they pile up in landfills and take years to decompose [10,11]. Therefore, recycling and reusing these separators significantly curtail the non-biodegradable battery waste [10]. Hence, there is an evident necessity for separator recycling and its re-utilization in batteries/capacitors [8,12–15].

Natarajan et al. [16] were the first to repurpose the spent LIB separator in metal-ion batteries. They have successfully utilized the recycled separator in a Li/LiMn<sub>2</sub>O<sub>4</sub> cell without sacrificing battery features. To date, relatively few reports only available on the upcycling of separators from spent LIBs. In this work, we are first to report the upcycling of the spent LIBs separators for SMBs to achieve superior electrochemical performance comparable with prevailing devices in safer and inexpensive ways. The separators are recycled through simple methods, and their physical properties are comparable with the commercial separators. We also report the direct reuse of these recycled polymer separators (RPS) to fabricate quasi-solid-state SMBs through a Na/RPS/Na<sub>2</sub>/3-Ni<sub>1/3</sub>Mn<sub>2/3</sub>O<sub>2</sub> assembly with 1 M sodium perchlorate (NaClO<sub>4</sub>) in ethylene carbonate (EC), dimethyl carbonate (DMC) and 5 % fluoroethylene carbonate (FEC) electrolyte solution. The fabricated Na/RPS/NNMO battery displayed promising electrochemical performance, including high capacity retention of 98 % and coulombic efficiency of 97 % over 100 cycles. The detailed results are discussed in the upcoming sections.

## 2. Experimental section

### 2.1. Recycling of polypropylene (PP) separator

First of all, the dead LIBs of mobile phones and laptops were collected from colleagues and electronics repair shops. Before dismantling, the spent batteries were fully discharged by immersing them overnight into a saturated sodium chloride solution. Then, the batteries were dismantled, and the separators were collected manually. The separator was immersed in deionized water and sonicated until the stuck cathodic and anodic particles were removed. Then, the separator was

washed manually several times and wiped with tissues, then dried in the oven for at least 6 h at 50 °C. The dried separators were cut into a circular shape of 19.5 mm diameter and kept in a 75 °C vacuum oven for 4 h. Then, these separators are transferred into an Ar-filled glove box (Mbraun, Germany, H<sub>2</sub>O < 0.1 ppm, and O<sub>2</sub> < 0.1 ppm) for cell fabrication.

### 2.2. Synthesis of P2-type Na<sub>2/3</sub>Ni<sub>1/3</sub>Mn<sub>2/3</sub>O<sub>2</sub> (NNMO)

NNMO was synthesized via the previously reported sol-gel method in a scalable way [17,18]. Sodium nitrate (NaNO<sub>3</sub>, >99 %, Sigma-Aldrich), nickel nitrate hexahydrate (Ni(NO<sub>3</sub>)<sub>2</sub>·6H<sub>2</sub>O, 99 %, Loba Chemie), manganese nitrate tetrahydrate (Mn(NO<sub>3</sub>)<sub>2</sub>·4H<sub>2</sub>O, 97 %, Sigma-Aldrich) in 2.08:1 M ratio was dissolved in deionized water to form a homogenous solution and kept for stirring in room temperature for 30 min. This solution was added dropwise to 20 mL of ethylene glycol (99.8 %, anhydrous, Sigma-Aldrich) under vigorous stirring. The obtained solution mixture was kept at 80 °C until the gel was formed. This gel precursor was heated in a tube furnace with a ramp rate of 3 °C min<sup>-1</sup> at 850 °C for 3 h and was allowed to cool naturally to ambient temperature to obtain the final product.

### 2.3. Structural characterization

The X-ray diffraction studies of NNMO were analyzed using Rigaku Smartlab automated multipurpose X-ray diffractometer with a monochromatic Cu K  $\alpha$  radiation ( $\lambda = 1.5604 \text{ \AA}$ ). The surface morphology of recycled separator and NNMO were imaged through field emission scanning electron microscopy (FE-SEM Gemini 560). The contact angle measurements of both recovered and fresh separators were performed using Holmarc's contact angle (HO-ED-M-01) by dropping 1 M NaClO<sub>4</sub> in EC: DMC and 5 % FEC electrolyte. Furthermore, a high-resolution transmission electron microscope (HR-TEM, JEM-2000, EX-II, JEOL, Japan) was used to acquire high-definition images of NNMO. Surface elemental mapping was determined by Energy-dispersive X-ray spectroscopy.

### 2.4. Wettability

A separator should have excellent electrolyte wettability to reduce the internal resistance, thereby attaining efficient ion transmission. The separator wettability is mainly analyzed by contact angle and electrolyte uptake measurements. The contact angle study provides information about the wetting speed of the electrolyte upon the separator, which depends on the separator structure. High electrolyte uptake facilitates fast ionic conductivity. The electrolyte uptake of the separator was measured by immersing it in the electrolyte and recording its weight at specific intervals. The electrolyte uptake and retention values were calculated by the following Equations 1 and 2,

$$\text{Electrolyte uptake (\%)} = (W_1 - W_0) / W_0 \times 100 \% \dots \dots \dots \text{Equation 1}$$

$$\text{Electrolyte retention (\%)} = (W_1 - W_0) / W_1 \times 100 \% \dots \dots \dots \text{Equation 2}$$

$W_0$  and  $W_1$  are the weights of the separators before and after immersing in the 1 M NaClO<sub>4</sub> in EC: DMC with 5 % FEC electrolyte, respectively [13,19].

## 2.5. Electrochemical characterization

### 2.5.1. Electrode fabrication

NNMO free-standing electrode film for the sodium-metal battery was handmade using mortar and pestle. Using ethanol as a solvent, the active material (NNMO), conductive carbon (acetylene black, AB), and binder (teflonized acetylene black, TAB-2) were taken in a ratio of 8:1:1 to form a thin film of NNMO. This film was further pressed onto a 14 mm stainless steel mesh (SS, Goodfellow, UK) current collector using a Specac hydraulic press (UK). Then, the electrodes are dried in a vacuum oven at 75 °C before cell fabrication for at least 4 h.

### 2.5.2. Electrolyte preparation

1 M sodium perchlorate ( $\text{NaClO}_4$ , Sigma-Aldrich, >98 %) dissolved in ethylene carbonate (EC, Sigma-Aldrich, >99 %) and dimethyl carbonate (DMC, anhydrous, Sigma-Aldrich, >99 %) in 1:1 vol% with 5 vol % of fluoroethylene carbonate (FEC, Sigma-Aldrich, >99 %) additive was used as the electrolyte. Electrolyte making and storing were done in an Ar-filled inert gas workstation ( $\text{H}_2\text{O} < 0.1$  ppm,  $\text{O}_2 < 0.1$  ppm).

### 2.5.3. Cell fabrication

Na/NNMO cell was fabricated in a 2016 coin-cell setup inside an Ar-filled inert gas workstation ( $\text{H}_2\text{O} < 0.1$  ppm,  $\text{O}_2 < 0.1$  ppm). For cell assembly with recycled polymer separators, ~75  $\mu\text{l}$  of 1 M  $\text{NaClO}_4$  in EC: DMC and 5 % FEC was used as the electrolyte. The NNMO electrode was placed on the cathode cap, and ~25  $\mu\text{l}$  of electrolyte was added, on which one separator was placed. After this, ~25  $\mu\text{l}$  electrolyte was added to the separator, and then the second separator was kept. Then, again, ~25  $\mu\text{l}$  electrolyte was added to the second separator on which sodium metal foil was placed and the cell was crimped. Then, the cells are taken outside the glove box for the electrochemical studies.

### 2.5.4. Ion-blocking cell fabrication

The ion-blocking cell was fabricated with 1 M  $\text{NaClO}_4$  in EC: DMC and 5 % FEC as the electrolyte in a 2016 coin cell assembly. A SS disk of 16 mm diameter was used as the ion-blocking electrode was placed on the cathode cap. Then, ~25  $\mu\text{l}$  each electrolyte was added to the SS mesh and between the two recycled separators, followed by placing an SS disk welded anode cap, which acts as the second blocking electrode, and the cell was crimped.

### 2.5.5. Na/stainless steel (SS) asymmetric cell fabrication for linear sweep voltammetry (LSV)

A Na/SS disk asymmetric cell was fabricated with 1 M  $\text{NaClO}_4$  in EC: DMC and 5 % FEC as the electrolyte in a 2016 coin cell. Sodium metal was placed on the cathode cap, and two recycled separators were kept above the metal. ~25  $\mu\text{l}$  of each electrolyte was added between the separators, then the SS disk welded anode cap was placed, and the cell was crimped.

### 2.5.6. Na/Na symmetric cell fabrication

A Na/Na symmetric cell was fabricated for sodium stripping-plating studies. First, sodium metal was placed on the top of the cathode cap, on which two recycled separators were kept. A total amount of ~75  $\mu\text{l}$  of electrolyte was added in between the separators, followed by the second sodium metal foil, and the cell was crimped.

## 3. Results and discussion

The XRD technique was used to analyze the crystallinity of the NNMO (Fig. S1, Supplementary Information). All peaks were sharp and well-defined, suggesting the high crystallinity of the as-synthesized NNMO sample. The XRD pattern of NNMO has a very sharp base peak at  $2\theta = 15^\circ$  representing the (002) plane. All peaks observed in the XRD pattern of NNMO can be indexed to hexagonal with space group 194: P63/mmc with lattice parameters:  $a = b = 2.88$  Å, and  $c = 11.15$  Å. The

surface morphology of RPS and NNMO was analyzed through FE-SEM. The commercial/fresh polymer separator (FPS) is also studied for comparison. Fig. 1a shows the FE-SEM images of the RPS, with a porous fiber-like nature, and FPS with similar morphology, which is given in Fig. 1b, where we can clearly distinguish the increased pore size of RPS. This expansion in pore radius may be attributed to the after-effect of the long cycling of spent batteries. SEM and HR-TEM images of plate-shaped NNMO arranged in stacks in different magnifications are given in Fig. 1d, e & f, respectively. Fig. 1c depicts the SAED pattern of NNMO with small spots in concentric circles corresponding to the polycrystallinity of the sample. Fig. 1g–j indicates the surface elemental composition of NNMO, where the presence of sodium, nickel, manganese, and oxygen is confirmed. The physical properties of FPS and RPS were analysed through BET measurements by cutting the separator into small pieces. Fig. S2 displays the nitrogen adsorption-desorption isotherm and pore distribution plot for FPS and RPS. The BET surface area = 113.83  $\text{m}^2 \text{g}^{-1}$  and pore radius = 19.67 Å obtained for RPS was much higher than FPS with surface area = 86.323  $\text{m}^2 \text{g}^{-1}$  and pore radius = 14.86 Å, which confirms the results obtained from SEM images.

Quick and uniformly dispersed absorbing ability of the electrolyte on the separator is highly beneficial to the fast and uniform transport of  $\text{Na}^+$  ions [7]. To understand the wettability of the separator, the contact angle measurement on RPS was performed using 1 M  $\text{NaClO}_4$  in EC: DMC and 5 % FEC solution. The image of the electrolyte on the RPS was captured immediately after adding a drop (Fig. 2 (a) RPS & (b) FPS), and the contact angle was measured using ImageJ software. The contact angle obtained for the RPS is  $30^\circ$ , indicating the best wettability, resulting in effective ion transport and reduced internal resistance. The contact angle of FPS was  $52^\circ$ , which was much higher than RPS, stating lower wettability because of the lower surface area and pore radius. The excellent wettability of the RPS can also be explained in terms of increased porosity, which agrees with the results obtained from SEM and BET analysis.

An ideal separator should possess excellent mechanical strength in order to ensure the safety of the battery when encountering burr, dendrites, and even an accidental crash [7,13,14]. Stress-strain studies were done to evaluate the mechanical strength and stability of our RPS and FPS (Fig. 2c). The RPS was observed to be robust enough to withstand high tension, with a tensile strength of 744 MPa and Young's modulus of 75 MPa, ensuring ultra-strong stability and additional safety to the SMB, whereas the FPS exhibited a tensile strength of 605 MPa with Young's modulus of 36 MPa. The breakpoint observed for FPS (21 %) was almost double that of RPS (11 %). In commercial cells, several post-treatment procedures were adopted, such as cross-linking, hot pressing, adding fillers, etc., to enhance the mechanical stability or tensile strength of the separators. It is very hard to predict the method adopted by the manufacturers to improve the mechanical properties of the separator. Also, the RPS underwent several cycles in the first life, but we used the untreated separator, FPS, for comparison. This may be the possible reason for the higher mechanical stability of the RPS than FPS.

The electrolyte uptake of the RPS and FPS immersed in 1 M  $\text{NaClO}_4$  in EC: DMC and 5 % FEC was studied at different time intervals from without immersing to 1, 5, 10, 15, 45, and 60 min immersing shown in Fig. 2d. The RPS exhibits the highest electrolyte uptake of 1152 %, significantly higher than the FPS, which is 357 % after 1 h (Table S1). We observed a steep increase in electrolyte uptake with increasing weight ratios as time progressed for the RPS, whereas the increase in FPS was slow and consistent. Similarly, the electrolyte retention obtained for RPS and FPS was 92 % and 78 % after 1 h soaking of separators in the electrolyte (Fig. S3). The excellent electrolyte uptake and retention for RPS are due to high porosity, better interfacial stability, and strong compatibility between the electrolyte and the separator, attributing to facile  $\text{Na}^+$ -ion transport channels for improving ionic conductivity.

The stability of electrolyte and RPS at higher voltage was investigated through LSV in a Na/SS asymmetric cell at a scan rate of 0.1  $\text{mV s}^{-1}$  from open circuit voltage (OCV) to 5 V vs. Na. The LSV of the cell



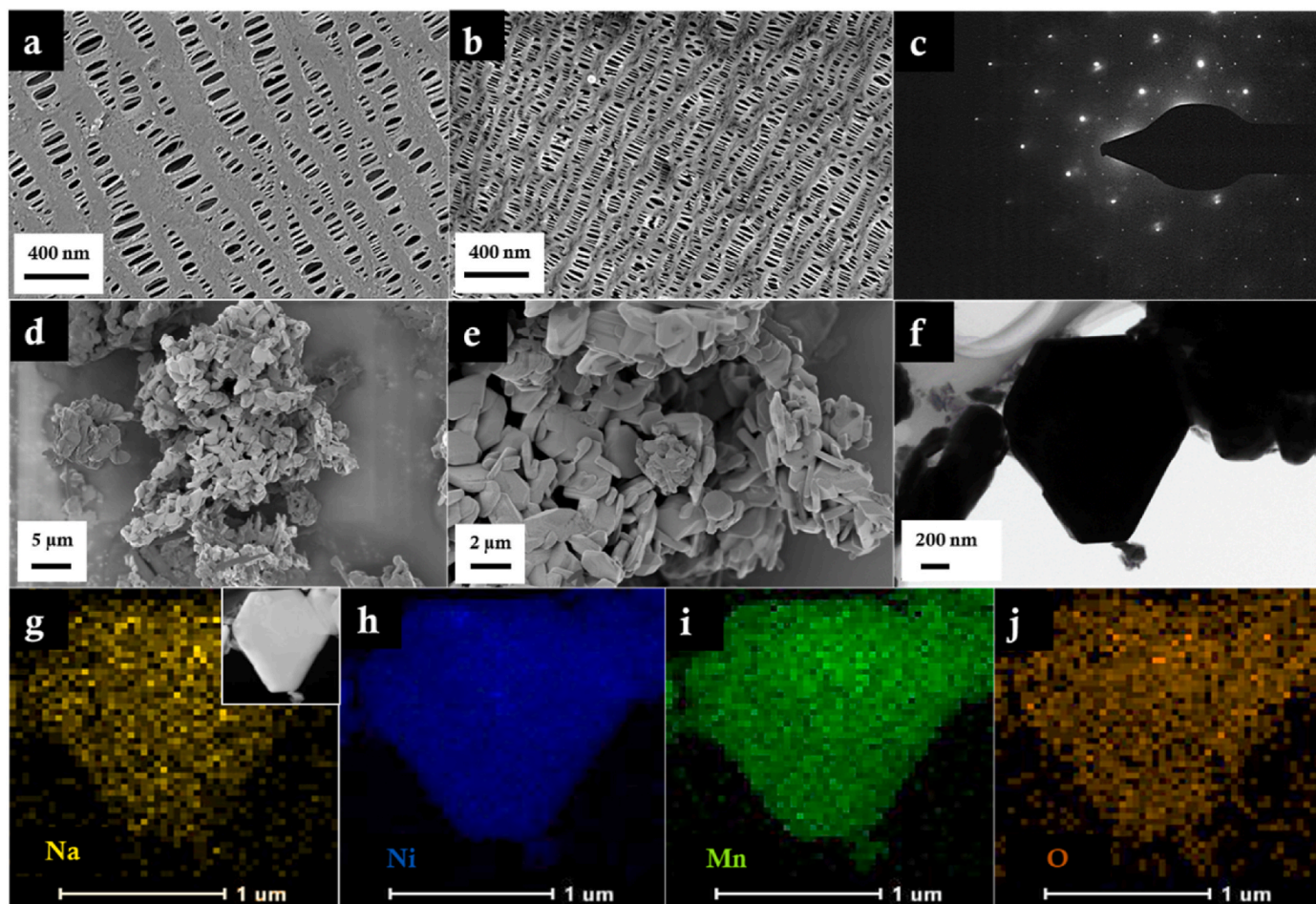


**Fig. 1.** Physical Characterization: FE-SEM images of (a) RPS, (b) FPS, (d & e) NNMO in two magnifications, (c) SEAD pattern of NNMO, (f) HR-TEM images of NNMO, EDAX mapping of NNMO: (g) Na, (h) Ni, (i) Mn, and (j) O.

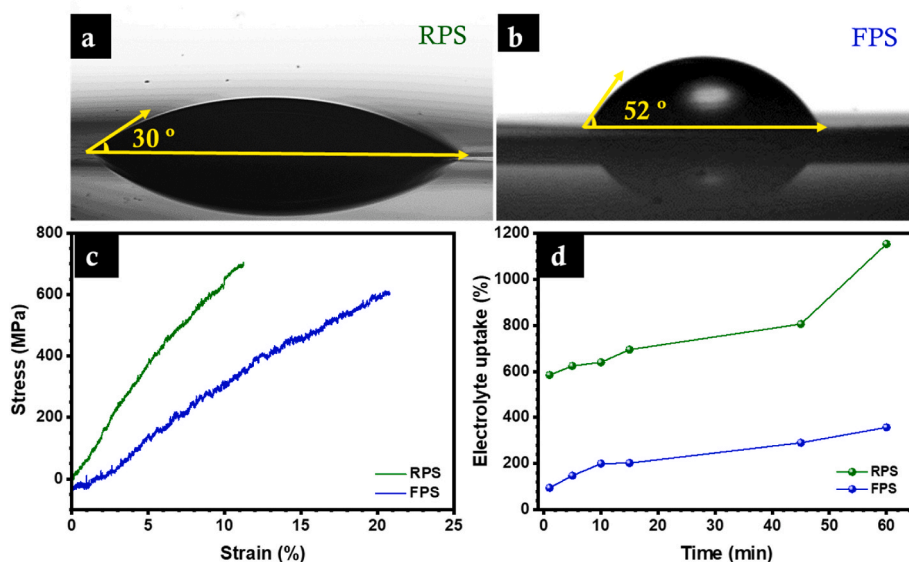


**Fig. 2.** Contact angle for 1 M NaClO<sub>4</sub> in EC: DMC +5 % FEC on (a) RPS, (b) FPS, (c) stress-strain curves for the separators, and (d) electrolyte uptake plot for the separators.

with 1 M NaClO<sub>4</sub> in EC: DMC and 5 % FEC electrolyte is shown in Fig. 3a. To examine the oxidation potential of the separator and the stability of the carbonate-based electrolyte, we analyzed its ability to avoid any redox reactions with changes in the cell potential. Any deviation in the

measured current with a change in potential indicates a reaction. We observed a spike in current at  $I = 0.01$  mA at a potential of  $V = 4.7$  V vs. Na for RPS, whereas Fig. S4 shows the LSV for FPS, where a spike in current is observed at  $I = 0.005$  mA at a potential of 4.7 V vs. Na

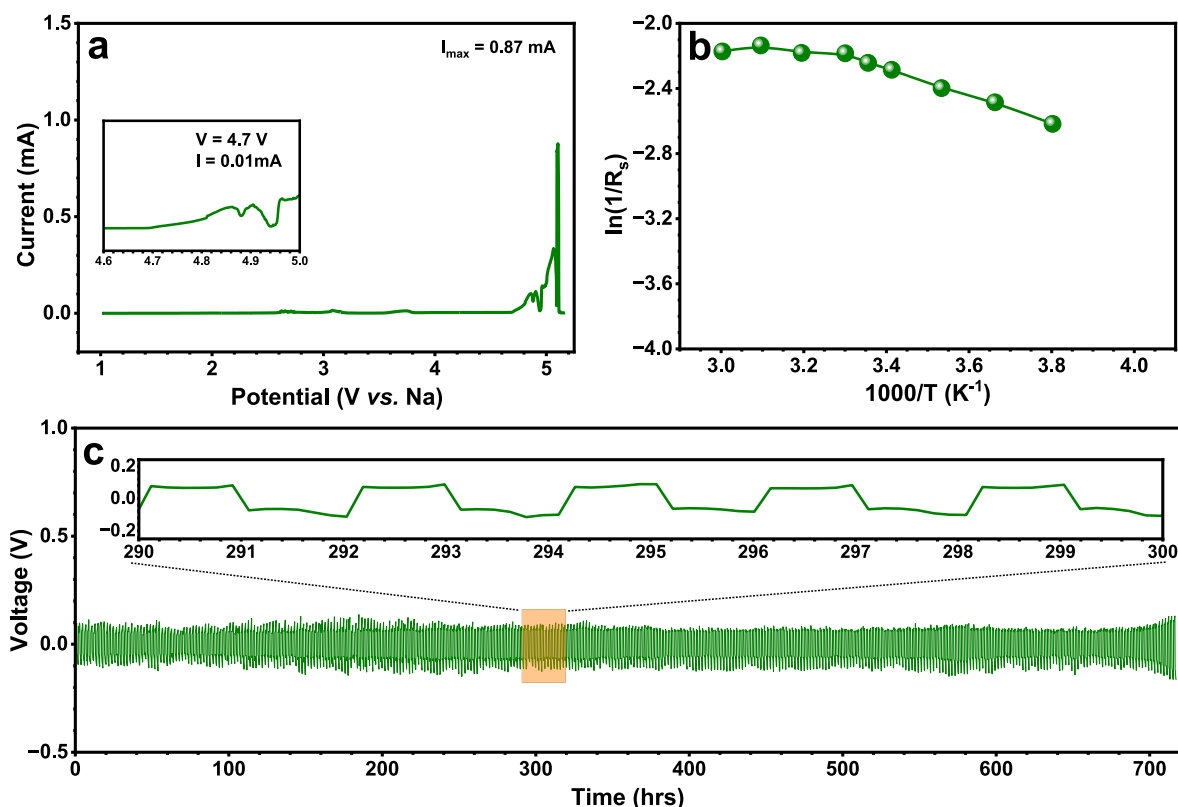


**Fig. 3.** (a) LSV analysis for Na/SS mesh asymmetric cell with 1 M NaClO<sub>4</sub> in EC: DMC + 5 % FEC electrolyte with RPS, (b) Arrhenius plot for ion blocking asymmetric cell with RPS, and (c) sodium stripping-plating GCD study of Na/Na symmetric cell with 1 M NaClO<sub>4</sub> in EC: DMC:5 % FEC electrolyte with FPS.

indicating that RPS exhibits almost similar decomposition profile of FPS. The stability of RPS is on par with FPS, suggesting that the RPS with carbonate-based electrolyte can be used in high voltage applications with higher stability. The RPS was able to withstand the changes in current at higher potentials, certifying the separator's high electrochemical stability and safety. Therefore, based on the above parameters, we have only continued the electrochemical studies with RPS.

In addition to the stability studies of the RPS and electrolyte, we have investigated their compatibility. In order to improve the stability and rate performance of the quasi-solid-state SMBs, the interfacial compatibility of the electrolyte-soaked separator with sodium metal electrode is significant. The separator should guarantee that it does not react with other battery components and maintain its structural integrity. The electrochemical impedance spectroscopy (EIS) with 1 M NaClO<sub>4</sub> in EC: DMC and 5 % FEC for RPS was performed in an ion-blocking cell. The bulk/solution resistance ( $R_s$ ) of the electrolyte-separator can be measured from the intercept of the Nyquist plot on the  $Z'$  axis. It was observed that the  $R_s$  of the RPS was 1.85  $\Omega$ , from which we calculated the conductance. The  $\ln$  (conductance,  $\sigma$ ) was plotted as a function of  $1000/T$ , as shown in Fig. 3b. The activation energy of the blocking cell with carbonate-based electrolyte using RPS can be calculated with the Arrhenius equation (Equation (3)) [15],

$$\sigma = \sigma_0 e^{-E_a/RT} \quad \text{Equation 3}$$

where  $\sigma_0$  is the absolute ionic conductivity,  $E_a$  is the activation energy,  $\sigma$  is the ionic conductivity,  $T$  is the temperature at which the impedance is recorded, and  $R$  is the universal gas constant. The slope of the plotted curve was found through the linear fit from which we calculated the activation energy 4.99 kJ mol<sup>-1</sup> for the cell with RPS. We observed that there was no prominent deviation in activation energy with a temperature change, suggesting that the carbonate-based electrolyte with RPS can be preferred in both low and high-temperature applications with excellent compatibility. The improved compatibility of the RPS with Na-

metal electrodes can be explained based on its excellent wettability and electrolyte retention, leading to effective Na-ion migration.

The interfacial stability between the RPS and sodium electrode was studied by a sodium periodic galvanostatic stripping-plating test with Na/separator-electrolyte/Na cell at a current density of 1 mA cm<sup>-2</sup>. Fig. 3c shows that the ion non-blocking cell with RPS exhibited a polarization potential of ~3 mV after 300 cycles and then increased to more than 30 mV after 700 cycles. The stable plating-stripping cycling and low polarization of the cell with RPS are due to the fast, consistent transfer of Na-ion. During the stripping-plating, the recycled separator sustained its integrity and robustness without causing separator failure for more than 600 h. The results further concluded that the RPS was able to retain the interfacial stability, thereby improving the cycle life and performance of the battery.

To further investigate the effectiveness of the RPS in the performance of the quasi-solid-state SMB, a cell was assembled with P2-type Na<sub>2</sub>/3Ni<sub>1/3</sub>Mn<sub>2/3</sub>O<sub>2</sub> as the cathode and sodium metal as the anode with RPS as the separator, and 1 M NaClO<sub>4</sub> in EC: DMC with 5 % FEC as the electrolyte. The electrochemical studies of Na/NNMO were carried out in a potential window of 2–3.95 V vs. Na. The cyclic voltammetry (CV) profile of Na/NNMO cells at different scan rates from 0.1 to 1 mV s<sup>-1</sup> is shown in Fig. 4a. Multiple CV peaks have been identified, suggesting the possibility of phase transition accompanying Na-insertion/de-insertion [17,20]. The redox peaks between 3 and 3.95 V vs. Na, which are prominent at lower scan rates, correspond to redox electronic pairs of Ni<sup>2+</sup>/Ni<sup>3+</sup> and Ni<sup>3+</sup>/Ni<sup>4+</sup> [18]. We observe peaks merging as the scan rate increases because of the fast diffusion of ions. Mn<sup>4+</sup> ions remain stable and electrochemically unreactive above 2 V vs. Na, which provides structural stability to the undistorted P2 hexagonal crystal structure due to the absence of Jahn-Teller active Mn<sup>3+</sup> ions [20]. The diffusion coefficient of Na<sup>+</sup> ions for the Na/NNMO cell with RPS was determined from the CV curves at different scan rates. The diffusion coefficient is calculated using the Randles-Sevcicks equation (Equation

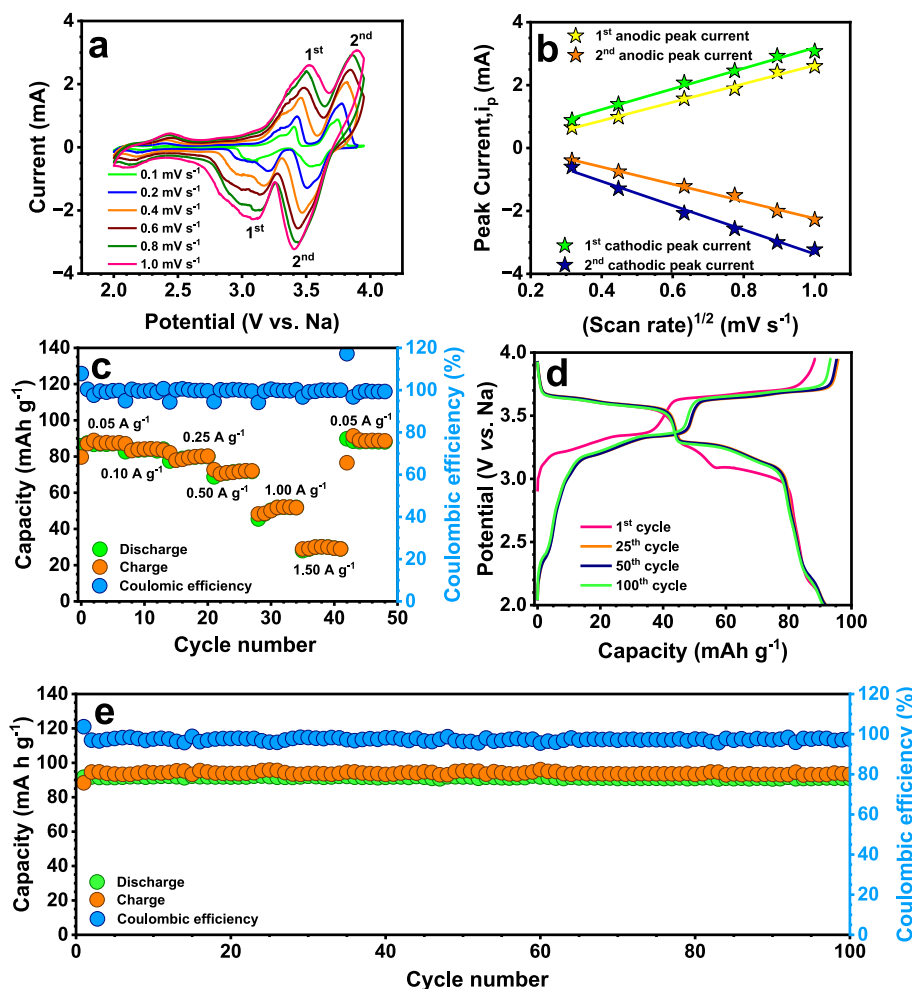


**Fig. 4.** Electrochemical studies of Na/RPS/NNMO cell: (a) CV curves at different scan rates, (b) diffusion coefficient plot, (c) rate performance at different current densities, (d) GCD curves for 1<sup>st</sup>, 25<sup>th</sup>, 50<sup>th</sup>, and 100<sup>th</sup> cycles, and (e) cycling profile at a current density of 0.05 A g<sup>-1</sup> from 2 to 3.95 V vs. Na over 100 cycles.

(4) [21],

$$i_p = 2.69 \times 10^5 n^{3/2} C_0 A D^{1/2} \nu^{1/2}$$

Equation 4

where  $D$  is the diffusion coefficient,  $i_p$  is the peak current,  $\nu$  is the scan rate,  $n$  is the number of Na<sup>+</sup> ions involved in the electrochemical reaction,  $C_0$  is the concentration of Na<sup>+</sup> ions, and  $A$  is the cross-sectional area of the electrode.

Fig. 4b represents the graph plotted with the peak current corresponding to the cathodic and anodic region vs. the square root of the scan rate, and the apparent diffusion coefficient is estimated from the slope of the curve. Fig. S5 shows the CV curves and corresponding diffusion coefficient plot of the Na/FPS/NNMO cell, and Table S2 shows the magnitude of both the anodic and cathodic diffusion coefficient for the Na/NNMO cell with RPS and FPS separator, where we clearly observed the increased diffusion coefficient of the cell with RPS. Additionally, the Na-diffusion coefficient is calculated from electrochemical impedance spectroscopy to support the studies conducted through CV and is depicted in Fig. S6.

The rate performance was evaluated with varying current rates from 0.05 to 1.5 A g<sup>-1</sup> Fig. 4c. The cell exhibited excellent rate performance at lower and higher current rates and retained a coulombic efficiency of >99 % even after high current cycling. The results indicate that RPS could sustain high current rates because of the high stability and robustness of the separator even after long cycling. Galvanostatic charge-discharge (GCD) curves for rate performance are shown in Fig. S7, from which a plateau and slope behavior similar to the CV

profile were observed. A long-term cycling profile was performed with RPS at 0.05 A g<sup>-1</sup> current from 2 to 3.95 V vs. Na (Fig. 4e). The cell displayed promising cycling stability and retained the initial discharge capacity of 91 mAh g<sup>-1</sup> to 98 % over 100 cycles with a coulombic efficiency of 97 %. GCD curves of the 1<sup>st</sup>, 25<sup>th</sup>, 50<sup>th</sup>, and 100<sup>th</sup> cycle are depicted in Fig. 4d, where we can clearly observe the overlapping of the discharge capacities, suggesting that the Na/RPS/NNMO cell can withstand the rigorous charge-discharge cycles, indicating the stability of the cell.

An *in-situ* impedance spectroscopy study (*in-situ* EIS) was conducted for the Na/RPS/NNMO cell to analyze the mechanism involved in the charge transfer reaction over a frequency region from 10 kHz to 1 Hz. Fig. 5 illustrates the detailed Nyquist plot of the changes in each potential during charge-discharge cycles. The charge transfer resistance ( $R_{CT}$ ) values decrease from 2 to 3.95 V vs. Na as the charging progresses. The de-sodiated state of NNMO exhibits lower  $R_{CT}$  values, indicating low resistance, which leads to faster diffusion of Na<sup>+</sup> ions with improved reaction kinetics. Meanwhile, in the discharging process, the  $R_{CT}$  values observed are much higher, suggesting a sluggish Na-ion diffusion process, and this continued throughout the cycling process, which was confirmed from the *in-situ* EIS plot up to 50 cycles. A similar pattern observed for up to 50 cycles clearly indicates that the RPS is compatible with Na-metal and NNMO cathodes in the quasi-solid state SMB.

#### 4. Conclusion

To summarise, the key objective of this study is to evaluate the



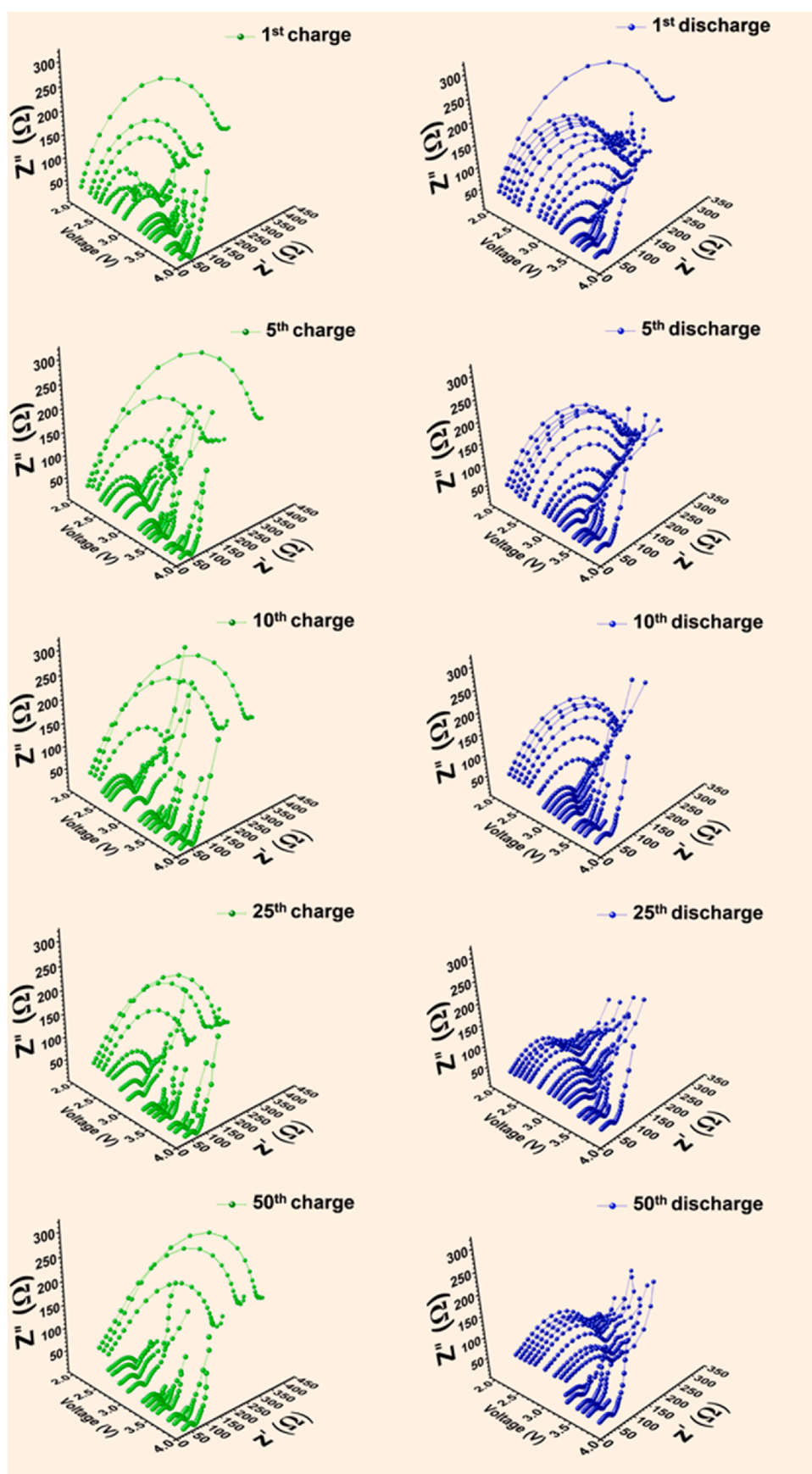


Fig. 5. *in-situ* EIS plots of Na/RPS/NNMO cell with impedance traces of 1<sup>st</sup>, 5<sup>th</sup>, 10<sup>th</sup>, 25<sup>th</sup>, and 50<sup>th</sup> charge-discharge at different potentials.

electrochemical performance of the RPS from dead Li-ion batteries in a carbonate-based electrolyte system for quasi-solid state Na-metal batteries. We observed that the RPS exhibits high wettability, surface area, and pore radius, resulting in efficient Na-ion transport and reduced internal resistance. The electrolyte uptake and retention values were obtained to be 1152 % and 92 %, respectively, indicating high porosity, better interfacial stability, and strong compatibility with the electrolyte. The recycled separator was robust enough to withstand high tension, with a tensile strength of 744 MPa and Young's modulus of 75 MPa, ensuring ultra-strong stability and additional safety to the SMB, with a breakpoint of 11 %. We observed no prominent deviation in activation energy with a temperature change, indicating that the carbonate-based electrolyte with RPS can be preferred in low and high-temperature applications with excellent compatibility. The assembled Na/RPS/NNMO battery displays promising electrochemical performance, including high capacity retention of 98 % and coulombic efficiency of 97 % after 100 cycles. The results validate the idea that the RPS can be used in low-cost, eco-friendly, high-current, and long-term large-scale applications in sodium batteries in a simple and sustainable recycling of dead Li-ion batteries.

#### CRediT authorship contribution statement

**Shaji Jyothilakshmi:** Conceptualization, Data curation, Formal analysis, Funding acquisition, Investigation, Writing – original draft, Writing – review & editing. **Krishnan Subramanyan:** Conceptualization, Data curation, Formal analysis, Funding acquisition, Investigation, Writing – review & editing. **Yun-Sung Lee:** Data curation, Funding acquisition, Project administration, Supervision, Validation, Writing – review & editing. **Vanchiappan Aravindan:** Writing – review & editing, Writing – original draft, Supervision, Project administration, Investigation, Funding acquisition, Formal analysis, Data curation, Conceptualization.

#### Declaration of competing interest

The authors declare that they have no known competing financial interests or personal relationships that could have appeared to influence the work reported in this paper.

#### Acknowledgement

The authors thank Santhan for recording the contact angle measurements. SJ thanks the Prime Minister's Research Fellowship (0902009) for financial support. KS thanks the Department of Science & Technology (DST), Govt. of India, for the financial support through the INSPIRE fellowship (IF180157). VA acknowledges financial support from the Anusandhan National Research Foundation (ANRF), Govt. of India, through Swarnajayanti Fellowship (SB/SJF/2020-21/12).

#### Appendix A. Supplementary data

Supplementary data to this article can be found online at <https://doi.org/10.1016/j.jpowsour.2025.237327>.

#### Data availability

Data will be made available on request.

#### References

- [1] S. Wang, B. Peng, J. Lu, Y. Jie, X. Li, Y. Pan, Y. Han, R. Cao, D. Xu, S. Jiao, Recent progress in rechargeable sodium metal batteries: a review, *Chem. Eur. J.* 29 (3) (2023) e202202380, <https://doi.org/10.1002/chem.202202380>.
- [2] B. Lee, E. Paek, D. Mitlin, S.W. Lee, Sodium metal anodes: emerging solutions to dendrite growth, *Chem. Rev.* 119 (8) (2019) 5416–5460, <https://doi.org/10.1021/acs.chemrev.8b00642>.
- [3] Y. Wang, Y. Wang, Y.X. Wang, X. Feng, W. Chen, X. Ai, H. Yang, Y. Cao, Developments and perspectives on emerging high-energy-density sodium-metal batteries, *Chem* 5 (10) (2019) 2547–2570, <https://doi.org/10.1016/j.chempr.2019.05.026>.
- [4] P. Arora, Z. John Zhang, Battery separators, *Chem. Rev.* 104 (10) (2004) 4419–4462, <https://doi.org/10.1021/cr020738u>.
- [5] S. Luiso, P. Fedkiw, Lithium-ion battery separators: recent developments and state of art, *Curr. Opin. Electrochem.* 20 (2020) 99–107, <https://doi.org/10.1016/j.coelec.2020.05.011>.
- [6] D.L. Thompson, J.M. Hartley, S.M. Lambert, M. Shiref, G.D.J. Harper, E. Kendrick, P. Anderson, K.S. Ryder, L. Gaines, A.P. Abbott, The importance of design in lithium ion battery Recycling-a critical review, *Green Chem.* 22 (22) (2020) 7585–7603, <https://doi.org/10.1039/d0gc02745f>.
- [7] L. Zhang, X. Li, M. Yang, W. Chen, High-safety separators for lithium-ion batteries and sodium-ion batteries: advances and perspective, *Energy Storage Mater.* 41 (June) (2021) 522–545, <https://doi.org/10.1016/j.ensm.2021.06.033>.
- [8] M. Bhar, U. Bhattacharjee, K. Yalamanchili, S.K. Martha, Effective upcycling of waste separator and boosting the electrochemical performance of recycled graphite anode for lithium-ion batteries, *J. Power Sources* 580 (July) (2023) 233403, <https://doi.org/10.1016/j.jpowsour.2023.233403>.
- [9] M.F. Lagadee, R. Zahn, V. Wood, Characterization and performance evaluation of lithium-ion battery separators, *Nat. Energy* 4 (1) (2019) 16–25, <https://doi.org/10.1038/s41560-018-0295-9>.
- [10] B. Huang, Z. Pan, X. Su, L. An, Recycling of lithium-ion batteries: recent advances and perspectives, *J. Power Sources* 399 (2018) 274–286, <https://doi.org/10.1016/j.jpowsour.2018.07.116>.
- [11] Y. Zhao, Y. Kang, J. Wozny, J. Lu, H. Du, C. Li, T. Li, F. Kang, N. Tavajohi, B. Li, Recycling of sodium-ion batteries, *Nat. Rev. Mater.* 8 (9) (2023) 623–634, <https://doi.org/10.1038/s41578-023-00574-w>.
- [12] S. Natarajan, K. Subramanyan, R.B. Dhanalakshmi, A.M. Stephan, V. Aravindan, Regeneration of polyolefin separators from spent Li-Ion battery for second life, *Batter. Supercaps* 3 (7) (2020) 581–586, <https://doi.org/10.1002/batt.202000024>.
- [13] J. Liu, J. Qin, Y. Mo, S. Wang, D. Han, M. Xiao, Y. Meng, Polyphenylene sulfide separator for high safety lithium-ion batteries, *J. Electrochem. Soc.* 166 (8) (2019) A1644–A1652, <https://doi.org/10.1149/2.1041908jes>.
- [14] X. Ma, Z. Cheng, T. Zhang, X. Zhang, Y. Ma, Y. Guo, X. Wang, Z. Zheng, Z. Hou, Z. Zi, High efficient recycling of glass fiber separator for sodium-ion batteries, *Ceram. Int.* 49 (14) (2023) 23598–23604, <https://doi.org/10.1016/j.ceramint.2023.04.194>.
- [15] K. Subramanyan, S. Jyothilakshmi, M. Ulaganathan, Y.-S. Lee, V. Aravindan, An efficient upcycling of graphite anode and separator for Na-Ion batteries via solvent-co-intercalation process, *Carbon* N. Y. 216 (2024) 118525, <https://doi.org/10.1016/j.carbon.2023.118525>.
- [16] S. Natarajan, K. Subramanyan, R.B. Dhanalakshmi, A.M. Stephan, V. Aravindan, Regeneration of polyolefin separators from spent Li-Ion battery for second life, *Batter. Supercaps* 3 (7) (2020) 581–586, <https://doi.org/10.1002/batt.202000024>.
- [17] Q. Liu, Z. Hu, M. Chen, C. Zou, H. Jin, S. Wang, Q. Gu, S. Chou, P2-Type Na<sub>2/3</sub>Ni<sub>1/3</sub>Mn<sub>2/3</sub>O<sub>2</sub> as a cathode material with high-rate and long-life for sodium ion storage, *J. Mater. Chem. A* 7 (15) (2019) 9215–9221, <https://doi.org/10.1039/c8ta11927a>.
- [18] K. Subramanyan, M.R. Palmurukan, Y.S. Lee, V. Aravindan, Exfoliated graphene oxide @ Sb<sub>2</sub>O<sub>3</sub> octahedrons as alloy-conversion anode for high-performance Na-ion batteries with P2-Type Na<sub>2/3</sub>Ni<sub>1/3</sub>Mn<sub>2/3</sub>O<sub>2</sub> cathode, *Electrochim. Acta* 470 (March) (2023) 143308, <https://doi.org/10.1016/j.electacta.2023.143308>.
- [19] Y.S. Wu, C.C. Yang, S.P. Luo, Y.L. Chen, C.N. Wei, S.J. Lue, PVDF-HFP/PET/PVDF-HFP composite membrane for lithium-ion power batteries, *Int. J. Hydrogen Energy* 42 (10) (2017) 6862–6875, <https://doi.org/10.1016/j.ijhydene.2016.11.201>.
- [20] Y. Wang, Y. Wang, Y. Xing, C. Jiang, Y. Pang, H. Liu, F. Wu, H. Gao, Entropy modulation strategy of P2-Type layered transition metal oxide cathodes for sodium-ion batteries with a high performance, *J. Mater. Chem. A* 11 (37) (2023) 19955–19964, <https://doi.org/10.1039/d3ta04094a>.
- [21] S. Jyothilakshmi, K. Subramanyan, Y.-S. Lee, V. Aravindan, Scalable synthesis of bulk TiO<sub>2</sub> hybrids toward efficient Li-Storage performance in “Rocking-Chair” type full-cell assembly with high voltage LiNi<sub>0.5</sub>Mn<sub>1.5</sub>O<sub>4</sub> cathode, *Adv. Mater. Technol.* 8 (12) (2023) 2202036, <https://doi.org/10.1002/admt.202202036>.